2804 *Chem. Mater.* **2010,** *22,* 2804–2813
DOI:10.1021/cm903735e

CHEMISTRY OF MATERIALS
Article

Monodisperse Octahedral α-MnS and MnO Nanoparticles by the Decomposition of Manganese Oleate in the Presence of Sulfur

Alessandra Puglisi,[†,‡] Sara Mondini,[†,‡] Simone Cenedese,[§,#] Anna M. Ferretti,[†] Nadia Santo,[⊥] and Alessandro Ponti*[,†,§]

[†]*Laboratorio di Nanotecnologie, Istituto di Scienze e Tecnologie Molecolari, Consiglio Nazionale delle Ricerche, via G. Fantoli 16/15, 20138 Milano, Italy,* [§]*Istituto di Scienze e Tecnologie Molecolari, Consiglio Nazionale delle Ricerche, via C. Golgi 19, 20133 Milano, Italy, and* [⊥]*Centro Interdipartimentale di Microscopia Avanzata, Università degli Studi di Milano, via G. Celoria 26, 20133 Milano, Italy.* [‡]*These authors contributed equally to this work.* [#]*Present address: Dipartimento di Chimica Fisica ed Elettrochimica, Università degli Studi di Milano, via C. Golgi 19, 20133 Milano, Italy*

Received December 12, 2009. Revised Manuscript Received January 28, 2010

Octahedral monodisperse α-MnS and MnO nanoparticles have been synthesized by decomposing manganese oleate and elemental sulfur in octadecene at high (250−320 °C) temperature. The chemical composition of the obtained NPs depends on the Mn:S ratio in an unexpected way. Pure α-MnS NP samples are obtained when S:Mn ≥ 2:1, whereas pure MnO NPs require S:Mn ≤ 0.6. Variation of several parameters (concentration of sulfur, heating rate and aging temperature and time) resulted in a α-MnS NP size interval of 11−14 (from Mn monooleate) and 18−30 nm (from Mn dioleate). For MnO NPs only, size control is also possible by addition of free oleic acid (14−24 nm). Analysis of TEM tilting experiments and electron diffraction shows that both α-MnS and MnO nanoparticles have octahedral shape and spontaneously form ordered arrays with strong texture in the {111} direction. Measurement of the magnetic properties showed that α-MnS nanoparticles consist of an antiferromagnetic core and a ferromagnetic-like shell that are exchange coupled below the blocking temperature of the shell (23 K for 29 nm α-MnS NP).

Introduction

Manganese(II) chalcogenides MnX (X = O, S, Se, Te) are antiferromagnetic (AFM) semiconductors. Upon descending the chemical group 16 from oxygen to tellurium, the band gap narrows and the Nèel temperature becomes higher (stronger AFM interactions).[1] MnS has received attention as a component of dilute magnetic semiconductors[2] and for short wavelength optoelectronic devices.[3] Whereas MnO crystallizes in a fcc structure, MnS can form three polymorphs: rocksalt structure α-MnS, zincblend structure β-MnS, and wurtzite structure γ-MnS. In the bulk, the α-phase is the most stable.[4] Submicrocrystals of α-MnS have attracted interest as an electrode material for Li-batteries,[5] and 1 μm α-MnS particles have been proposed as a catalyst for carbon fixation in the prebiotic world.[6] Because of the peculiar properties of α-MnS, several groups reported upon micro- or nanostructures made of α-MnS. Microparticles of α-MnS have been obtained by hydrothermal,[7] solvothermal,[8] and biomolecule-assisted[9] methods. One-dimensional α-MnS nanostructures (wires or belts) have been obtained by solvothermal,[10] hydrothermal,[11] and CVD[3,12,13] methods. Of course, α-MnS nanoparticles (NPs) also deserved some attention. Monodisperse 20−80 nm α-MnS NPs have been synthesized from $MnCl_2$ and bis-(trimethylsilyl)sulfide in TOP/TOPO but their morphology suggested that they were aggregates of finer particles.[1] NPs of α-, β-, and γ-MnS have been synthesized by decomposing a Mn dithiocarbamate precursor, source of both Mn and S, in hexadecylamine.[14] Control over the crystal phase was achieved by changing the reaction temperature, and α-MnS NPs (∼30 nm) were obtained at 250 °C. A similar precursor (Mn alkyl xanthate) dissolved in trioctylamine was used to synthesize

*Corresponding author.

(1) Kan, S. H.; Felner, I.; Banin, U. *Isr. J. Chem.* **2001**, *41*, 55–61.
(2) Furdyna, J. K.; Samarth, N. *J. Appl. Phys.* **1987**, *61*, 3526–3531.
(3) Kim, D. S.; Lee, J. Y.; Na, C. W.; Yoon, S. W.; Kim, S. Y.; Park, J.; Jo, Y.; Jung, M. H. *J. Phys. Chem. B* **2006**, *110*, 18262–18266.
(4) Skromme, B. J.; Zhang, Y.; Smith, D. J.; Sivananthan, S. *Appl. Phys. Lett.* **1995**, *67*, 2690–2692.
(5) Zhang, N.; Yi, R.; Wang, Z.; Shi, R. R.; Wang, H. D.; Qiu, G. Z.; Liu, X. H. *Mater. Chem. Phys.* **2008**, *111*, 13–16.
(6) Zhang, X. V.; Martin, S. T.; Friend, C. M.; Schoonen, M. A. A.; Holland, H. D. *J. Am. Chem. Soc.* **2004**, *126*, 11247–11253.
(7) Michel, F. M.; Schoonen, M. A. A.; Zhang, X. V.; Martin, S. T.; Parise, J. B. *Chem. Mater.* **2006**, *18*, 1726–1736.
(8) Biswas, S.; Kar, S.; Chaudhuri, S. *J. Cryst. Growth* **2005**, *284*, 129–135.
(9) Jiang, J. H.; Yu, R. N.; Zhu, J. Y.; Yi, R.; Qiu, G. Z.; He, Y. H.; Liu, X. H. *Mater. Chem. Phys.* **2009**, *115*, 502–506.
(10) Ma, D. K.; Huang, S. M.; Zhang, L. J. *Chem. Phys. Lett.* **2008**, *462*, 96–99.
(11) An, C. H.; Tang, K. B.; Liu, X. M.; Li, F. Q.; Zhou, G.; Qian, Y. T. *J. Cryst. Growth* **2003**, *252*, 575–580.
(12) Ge, J. P.; Li, Y. D. *Chem. Commun.* **2003**, 2498–2499.
(13) Ge, J. P.; Wang, J.; Zhang, H. X.; Li, Y. D. *Chem. Eur. J.* **2004**, *10*, 3525–3530.
(14) Jun, Y. W.; Jung, Y. Y.; Cheon, J. *J. Am. Chem. Soc.* **2002**, *124*, 615–619.

 Published on Web 03/24/2010

α-MnS NPs at 150 °C.[15] Another single precursor (a Mn diamino diphenylthiocarboxylate) in oleylamine/octadecene was used to produce monodisperse α-MnS NPs at temperatures in the 300−350 °C range.[16] Much simpler precursors ($MnCl_2$ and elemental S) dissolved in oleylamine and reacted at high temperature gave γ-MnS NPs.[17] Different shapes were obtained by changing reaction temperature and the Mn:S ratio, the latter not being feasible when a single precursor is used. Very recently, the use of Mn oleate has been introduced to synthesize MnS NPs.[18] Mn oleate dissolved in a 1:1 mixture of oleylamine and dodecanethiol (the source of S) treated at 280 °C for 1 h afforded 11 nm MnS NPs. The use of metal oleates to synthesize metal oxide NPs was introduced in 2004 by Peng[19] and Hyeon[20] groups as a consequence of the fact that iron oleate is the actual precursor in the synthesis of iron oxide NPs by the decomposition of $Fe(CO)_5$ in the presence of oleic acid (OlAc).[21] Mn oleate[22−27] and stearate[28] have been mostly employed as a precursor in the synthesis of MnO NPs. Decomposing Mn oleate in a hydrocarbon solvent at high temperature yields monodisperse MnO NPs, which often have a faceted profile,[26,27,29] a morphology also observed using Mn stearate,[28] Mn acetylacetonate,[30,31] and Mn acetate.[32]

First, we synthesized two precursors, namely, manganese dioleate [$Mn(Ol)_2$] and manganese monooleate (hydr)oxide [Mn(OH)(Ol)]. Next, we investigated the synthesis of MnS NPs using the two-precursor systems $Mn(Ol)_2$/S and Mn(OH)(Ol)/S. These afford complete flexibility in the choice of the Mn:S ratio. At variance with previous syntheses of MnS NPs, we do not employ the surfactant as solvent. Rather, we use a noncoordinating hydrocarbon solvent such as octadecene and the surfactant is part of the metal precursor. The metal-surfactant ratio can be thus varied by adding free surfactant, but such ratio cannot be lower than 1 for Mn(OH)(Ol) or 2 for $Mn(Ol)_2$. The chemical composition of the NPs (MnS or MnO) depends in an unexpected way on the Mn:S ratio, and the morphology of the NPs depends the nature of the Mn oleate precursor, the Mn:S ratio, the reaction temperature and time, and the heating rate. Analysis of TEM imaging and diffraction data showed that both MnS and MnO NPs have octahedral shape and can spontaneously form strongly textured ordered arrays. Finally, MnS NPs comprise regions with different magnetic behavior.

Experimental Section

Manganese(II) chloride (99+%), tetramethylammonium hydroxide pentahydrate, piperidine, sulfur powder (99.98%), oleic acid (reagent grade, 99%), stearic acid (Grade I, approximately 99%), and octadecene (purum, ≥95.0%) were purchased from Sigma-Aldrich and used as received without further purification.

Synthesis of Manganese Distearate [$Mn(St)_2$].[28] Stearic acid (2.84 g., 10 mmol) was dissolved in 15 mL of MeOH and heated to 60 °C until it became a clear solution, which was then allowed to cool to room temperature. A solution of tetramethylammonium hydroxide (TMAOH, 1.81 g, 10 mmol) in MeOH (5 mL) was added and the resulting clear mixture was allowed to stir for 15 min, to ensure the reaction to go to completion. To this solution was added $MnCl_2$ (0.63 g, 5 mmol) dissolved in MeOH (5 mL) dropwise with vigorous stirring: a white precipitate of $Mn(St)_2$ slowly flocculated. The precipitate was filtered, repeatedly washed with cold methanol, and dried under vacuum to afford 2.32 g (3.73 mmol, 75% yield) of $Mn(St)_2$ as a white powdery solid. IR (thin film on NaCl), ν (cm^{-1}): 2955, 2918, 2849, 1560, 1472, 1464, 1435, 718. ESI-MS: 622.474 (MH^+).

Synthesis of Manganese Dioleate [$Mn(Ol)_2$]. $Mn(Ol)_2$ was synthesized modifying the above method for $Mn(St)_2$. To a stirred solution of oleic acid (2.82 g, 10 mmol) in MeOH (15 mL), tetramethylammonium hydroxide (1.81 g, 10 mmol) dissolved in MeOH (5 mL) was added. After the addition, the clear solution was stirred for 15 min. Then a solution of $MnCl_2$ (0.63 g, 5 mmol) in MeOH (5 mL) was slowly added through a syringe. A light pink precipitate immediately formed. Several attempts to isolate the product by filtration were not successful. The crude mixture was then evaporated under reduced pressure, taken up in hexane (30 mL) and washed with 30 mL of water. The organic phase was dried over $MgSO_4$ and evaporated to afford the product as a light-pink foamy solid in quantitative yield. IR (thin film on NaCl), ν (cm^{-1}): 2959, 2925, 2874, 2860, 1552, 1467, 1460, 1379, 724. ESI-MS: 618.441 (MH^+), 640.424 (MNa^+).

Synthesis of Manganese Monooleate (hydr)oxide [Mn(OH)(Ol)]. Mn(OH)(Ol) was synthesized modifying a literature method for manganese monolaurate.[33] To a vigorously stirred solution of oleic acid (2.26 g, 8 mmol) in MeOH (100 mL), $MnCl_2$ (1.01 g, 8 mmol) was added. To this clear solution was slowly added piperidine (2.37 mL, 24 mmol) dissolved in MeOH

(15) Pradhan, N.; Katz, B.; Efrima, S. *J. Phys. Chem. B* **2003**, *107*, 13843–13854.
(16) Tian, L.; Yep, L. Y.; Ong, T. T.; Yi, J. B.; Ding, J.; Vittal, J. J. *Cryst. Growth Des.* **2009**, *9*, 352–357.
(17) Joo, J.; Na, H. B.; Yu, T.; Yu, J. H.; Kim, Y. W.; Wu, F. X.; Zhang, J. Z.; Hyeon, T. *J. Am. Chem. Soc.* **2003**, *125*, 11100–11105.
(18) Choi, S. H.; An, K.; Kim, E. G.; Yu, J. H.; Kim, J. H.; Hyeon, T. *Adv. Funct. Mater.* **2009**, *19*, 1645–1649.
(19) Jana, N. R.; Chen, Y. F.; Peng, X. G. *Chem. Mater.* **2004**, *16*, 3931–3935.
(20) Park, J.; An, K. J.; Hwang, Y. S.; Park, J. G.; Noh, H. J.; Kim, J. Y.; Park, J. H.; Hwang, N. M.; Hyeon, T. *Nat. Mater.* **2004**, *3*, 891–895.
(21) Hyeon, T.; Lee, S. S.; Park, J.; Chung, Y.; Bin Na, H. *J. Am. Chem. Soc.* **2001**, *123*, 12798–12801.
(22) Na, H. B.; Lee, J. H.; An, K. J.; Park, Y. I.; Park, M.; Lee, I. S.; Nam, D. H.; Kim, S. T.; Kim, S. H.; Kim, S. W.; Lim, K. H.; Kim, K. S.; Kim, S. O.; Hyeon, T. *Angew. Chem., Int. Ed.* **2007**, *46*, 5397–5401.
(23) Berkowitz, A. E.; Rodriguez, G. F.; Hong, J. I.; An, K.; Hyeon, T.; Agarwal, N.; Smith, D. J.; Fullerton, E. E. *J. Phys. D: Appl. Phys.* **2008**, 134007.
(24) Berkowitz, A. E.; Rodriguez, G. F.; Hong, J. I.; An, K.; Hyeon, T.; Agarwal, N.; Smith, D. J.; Fullerton, E. E. *Phys. Rev. B* **2008**, *77*, 024403.
(25) Pan, D. P. J.; Senpan, A.; Caruthers, S. D.; Williams, T. A.; Scott, M. J.; Gaffney, P. J.; Wickline, S. A.; Lanza, G. M. *Chem. Commun.* **2009**, 3234–3236.
(26) Li, Q.; Wang, J.; He, Y. J.; Liu, W.; Qiu, X. H. *Cryst. Growth Des.* **2009**, *9*, 3100–3103.
(27) Schladt, T. D.; Graf, T.; Tremel, W. *Chem. Mater.* **2009**, *21*, 3183–3190.
(28) Chen, Y. F.; Johnson, E.; Peng, X. G. *J. Am. Chem. Soc.* **2007**, *129*, 10937–10947.
(29) Lee, S. Y.; Harris, M. T. *J. Colloid Interface Sci.* **2006**, *293*, 401–408.
(30) Seo, W. S.; Jo, H. H.; Lee, K.; Kim, B.; Oh, S. J.; Park, J. T. *Angew. Chem., Int. Ed.* **2004**, *43*, 1115–1117.
(31) Si, H. L.; Wang, H. Z.; Shen, H. B.; Zhou, C. H.; Li, S.; Lou, S. Y.; Xu, W. W.; Du, Z. L.; Li, L. S. *CrystEngComm* **2009**, *11*, 1128–1132.
(32) Yin, M.; O'Brien, S. *J. Am. Chem. Soc.* **2003**, *125*, 10180–10181.
(33) Malik, A. S.; Duncan, M. J.; Bruce, P. G. *J. Mater. Chem.* **2003**, *13*, 2123–2126.

Scheme 1

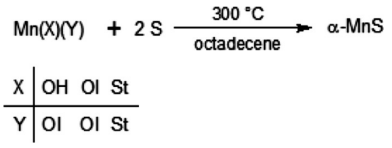

(100 mL) through a funnel. The solution turned light yellow and then dark brown. After 12 h aging, MeOH was decanted off and the dark slurry residue was taken up in hexane (50 mL) and washed with water (50 mL). The organic phase was dried over $MgSO_4$ and evaporated to afford 1.98 g of the desired product as a dark solid (70% yield). IR (thin film on NaCl), ν (cm^{-1}): 2959, 2925, 2874, 2860, 1541, 1466, 1459, 1378. ESI-MS: 354.196 (MH^+), 376.178 (MNa^+).

Conventional Synthesis of Manganese Oleate. Manganese oleate was prepared by the conventional method reported in ref 20. IR (thin film on NaCl), ν (cm^{-1}): 3006, 2926, 2855, 1553, 1419, 1312, 722.

Typical Synthesis of α-MnS NPs. 1.25 mmol (0.25 M) of the appropriate precursor and 80 mg (2.5 mmol, 0.5 M) of S were added to 5 mL of octadecene (see Scheme 1). The reaction mixture was subjected to three vacuum-Ar cycles at room temperature, and then heated to 120 °C while degassing by bubbling Ar. It was subjected to three vacuum-Ar cycles and further degassed for 15 min at 120 °C.

The mixture was then heated to 300 °C at a rate of 10 °C/min using a programmable heating unit. The dark green mixture was aged at that temperature for 30 min and then cooled to RT. The NPs were precipitated by addition of a 1:1 acetone:EtOH mixture (20 mL) and collected by centrifugation. The NPs were dispersed in hexane (5 mL) and the above procedure was repeated 2 times. The NPs could be easily dispersed in apolar solvents like hexane and toluene.

Other Syntheses of α-MnS NPs. The above procedure has been varied as to the following conditions: S:Mn ratio, heating rate, aging temperature and time, addition of free OlAc.

Synthesis of MnO NPs. The synthesis of MnO NPs is identical to that for α-MnS NPs except for the amount of sulfur. MnO NPs were obtained either in the absence of sulfur and adding sulfur up to a S:Mn ratio of 0.6:1. Besides, the effect of adding free oleic acid up to ~4 equiv. wrt Mn was studied.

Characterization. For TEM characterization, a drop of NP dispersion was placed on a Formvar/carbon-coated or on a holey-carbon copper grid and dried under argon. The sample grids were examined by an EFTEM LEO 912AB 120 kV microscope or by a FEI Tecnai G2 F20 200 kV microscope (for HRTEM). The diameter of the NPs was obtained from the TEM images by analyzing them by means of a computer program developed in our lab. Each NP image is fitted to a photometric model without human intervention thus resulting in a quick, unbiased, reproducible measurement of the NP morphology. Several hundred NP models were fitted for each sample, and the resulting best-fit values were subjected to statistical analysis. For XRD measurements, the NP dispersion was deposited on a background-free silica sample holder and air-dried. X-ray diffractograms were collected using a Philips PW 1820 diffractometer using CuK_α radiation, a graphite monochromator on diffracted beam, and a scintillation counter. Rietveld refining was performed by Maud (Materials Analysis Using Diffraction) analysis program.[34] For the measurement of magnetic properties, a weighted amount of precipitated and dried NPs was placed in a gel capsule. The sample was first cooled to 5 K in zero field and the ZFC magnetization was measured applying a 100 Oe field and heating the sample to 300 K. The sample was then cooled to 5 K in a 100 Oe field and the FC magnetization measured as before. Hysteresis loops were measured at 5 K after field cooling at 50 kOe. Magnetic measurements were carried out by a Quantum Design MPMS-5 SQUID magnetometer.

(34) Lutterotti, L.; Matthies, S.; Wenk, H.-R. In *Proceedings of the Twelfth International Conference on Textures of Materials*; Montreal, Aug 9−13, 1999; National Research Council of Canada: Ottawa, ON, 1999; Vol. *1*, p 1599.

Results and Discussion

Precursors. The conventional procedure to prepare manganese oleate involves the addition of a base to a 1:2 Mn:OlAc solution to yield a deep red solid,[19] or the reaction of manganese chloride (1 equiv.) with sodium oleate (2 equiv.) to afford a waxy sticky solid.[20] In both cases, the hydroalcoholic solution where the reaction between Mn and oleate takes place is in contact with hexane which quickly extracts the product. Even though in a single case[22] Mn oleate is described as a pink powder, all reports in the literature refer to a solid dark compound. The saturated analogous Mn distearate can be synthesized in pure form as a white powder only when a manganese chloride solution (1 equiv.) is added dropwise to a fresh solution of tetramethylammonium (TMA) stearate (2 equiv.).[28] If TMAOH is added to the manganese chloride/stearic acid solution, a brownish product is obtained that contains some (hydr)oxidic impurity. Furthermore, manganese monolaurate (hydr)oxide has been synthesized[33] as a brown, amorphous solid by adding piperidine to a 1:1 (manganese chloride):(lauric acid) solution. On the basis of such reports, one may wonder that even though the used Mn:Ol ratio is 1:2, the conventionally prepared dark manganese oleate could be a mixture of manganese dioleate ($Mn(Ol)_2$) and manganese monooleate (hydr)oxide [Mn(OH)(Ol)]. Indeed, hexane can extract both Mn(OH)(Ol) and $Mn(Ol)_2$ because both products are much more soluble in hexane than in an hydroalcoholic medium. Furthermore, Mn(II) salts are prone to hydrolysis[33] and/or oxidation by atmospheric oxygen.[35]

We were thus prompted to synthesize and use as NP precursors manganese dioleate [$Mn(Ol)_2$] and manganese monooleate (hydr)oxide [Mn(OH)(Ol)]. As described in the Experimental Section, we made some effort to prepare both $Mn(Ol)_2$ and Mn(OH)(Ol) as pure as possible, even if these compounds could not be filtered, crystallized nor separated by chromatography on silica gel. The obtained $Mn(Ol)_2$ is slightly pink while Mn(OH)(Ol) is dark brown. The IR spectrum of both products shows the characteristic band of the carboxylate moiety (see the Supporting Information). The ESI-MS spectra (see the Supporting Information) of the manganese precursors prepared by the conventional and the presently proposed methods display a similar set of peaks corresponding to

(35) Tian, Z. R.; Tong, W.; Wang, J. Y.; Duan, N. G.; Krishnan, V. V.; Suib, S. L. *Science* **1997**, *276*, 926–930.

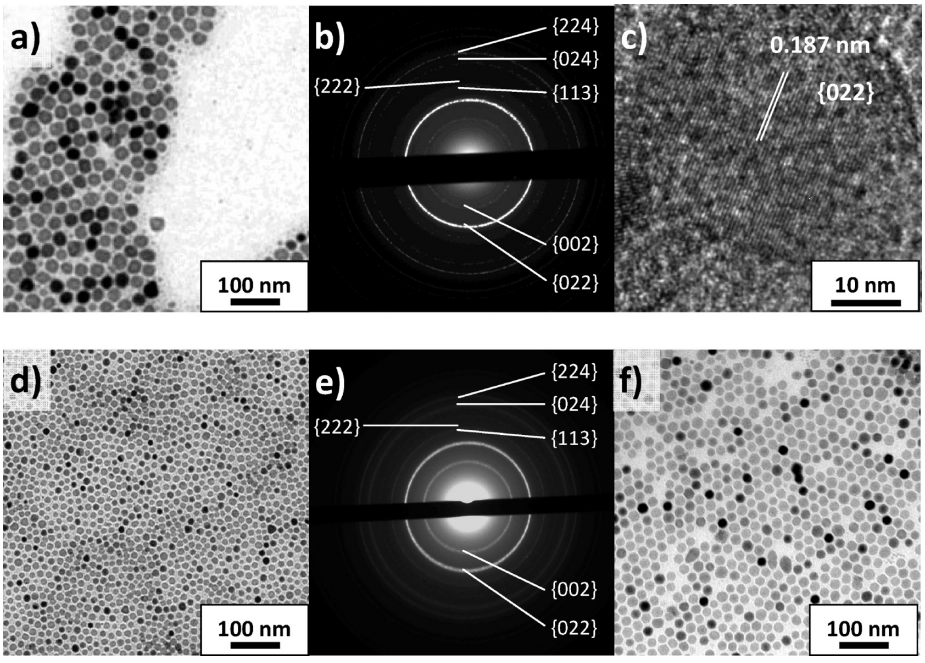

Figure 1. α-MnS NPs synthesized with either precursor using typical reaction conditions, except when otherwise noted. 30 nm α-MnS NPs from $Mn(Ol)_2$ precursor: (a) TEM image, (b) electron diffraction pattern, (c) HRTEM image displaying the {022} planes of α-MnS separated by 0.185 nm. 14 nm α-MnS NPs from Mn(OH)(Ol) precursor: (d) TEM image, (e) electron diffraction pattern. (f) 21 nm α-MnS NPs from $Mn(Ol)_2$ precursor, aging temperature 320 K.

the $[Mn(Ol)_2H]^+$ ($m/z = 618.4$) and $[Mn(Ol)_2Na]^+$ ($m/z = 640.4$) ions, and the $[Mn(OH)(Ol)H]^+$ ion ($m/z = 354.2$). Besides, peaks related to $[Mn(Ol)(OMe)H]^+$ ($m/z = 368.2$) are present that arise from the reaction of the manganese compounds with MeOH, which is needed to prepare the solution for injection in the ESI-MS apparatus. The compounds are differentiated by the ESI peak intensity. The intensity of the monooleate peaks with respect to those of the dioleate peaks dramatically grows from $Mn(Ol)_2$ to the conventionally prepared compound, to Mn(OH)(Ol).

Hence, the described syntheses produce a mixture of two products but enriched in the desired compound with respect to the conventionally prepared precursor. This conclusion is further confirmed by the consistently different synthetic outcome observed when either compound is used as a NP precursor.

Synthesis of α-MnS NPs. Monodisperse NPs of α-MnS synthesized using either precursor under typical conditions (see the Experimental Section) are shown in Figure 1a−e. The NPs are monocrystals (cfr Figure 1c) with hexagonal profile. The electron diffraction (ED) and the X-ray diffraction (XRD) patterns in Figures 1 and 2 show that the NPs have the fcc α-MnS structure. The XRD profiles could be well-reproduced by the Rietveld method. The refinement resulted in crystallite diameters a little larger than the values from the analysis of TEM images, thus confirming the single-crystal nature of the NPs.

There is a substantial size difference between NPs synthesized from the two precursors (Figure 1). When using $Mn(Ol)_2$ the NPs have median diameter $\langle d \rangle = 29$ nm and diameter standard deviation $\sigma = 3$ nm, whereas use of Mn(OH)(Ol) results in NPs with $\langle d \rangle = 14$ nm and $\sigma = 1.7$ nm. This size difference is almost always observed: under the same reaction conditions, NPs from $Mn(Ol)_2$ are about twice as large as those from Mn(OH)(Ol) (Table 1), with the only exception of brief low-temperature aging.

Figure 3 reports the variation in median diameter (solid lines) and dispersion ratio $\sigma/\langle d \rangle$ (dashed lines) with aging temperature T_{ag} or time t_{ag}. The NPs are larger at higher T_{ag}. There is a single exception in that NPs from $Mn(Ol)_2$ are smaller when aged at $T_{ag} = 320$ °C rather than at 300 °C (see also Figure 1f). The dispersion ratio $\sigma/< d >$ is generally lower at higher T_{ag}. For Mn(OH)(Ol), there is a minimum at about 300 °C, whereas for $Mn(Ol)_2$, the lowest dispersion is at 320 °C. The duration t_{ag} of aging is of critical importance to obtain monodisperse NPs.[16] At longer t_{ag} the size dispersion is lower, particularly at $T_{ag} = 320$ °C. On the contrary, the NP size is barely affected by the duration of aging period, particularly at higher T_{ag}. The NPs have formed and grown to almost their ultimate size during the heating period and grow very little during the aging period.

To clarify this issue, we analyzed the NP content of reaction mixture aliquots drawn during the heating step. As shown in Figure 4, though polydisperse and irregularly shaped, NPs are already about 10 nm in diameter when the ramping temperature is as low as 250 °C. This agrees with the observation that conventionally prepared Mn oleate begins to decompose at 200−230 °C.[27]

Lowering the heating rate from typical 10 °C/min to 5 or 3 °C/min makes the NPs slightly larger but the resulting dispersion is rather high (> 15%). To investigate the effect of a faster rate, NPs have been synthesized by

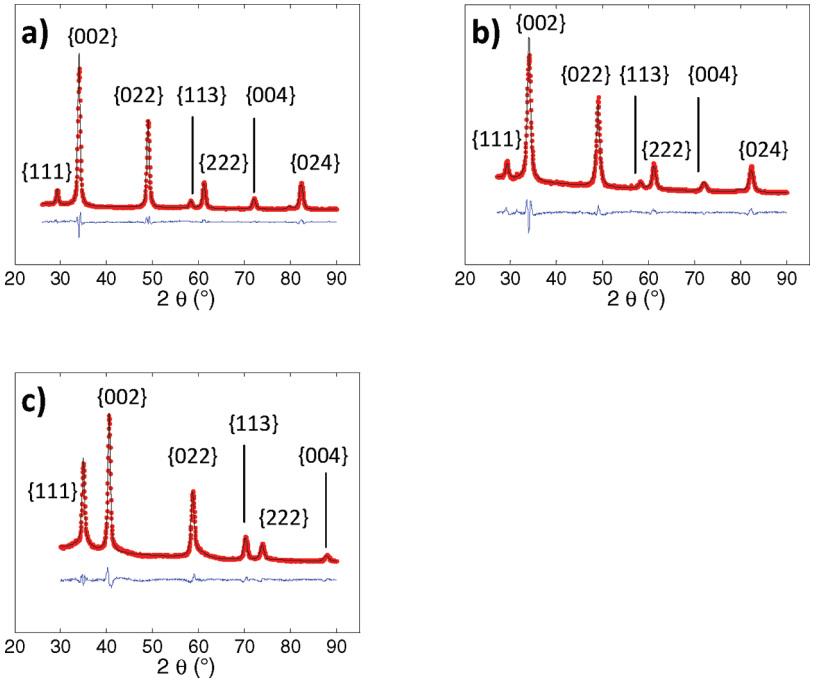

Figure 2. Rietveld refinement of the XRD patterns of α-MnS and MnO NPs synthesized under typical reaction conditions. Red dots, experimental; black line, refined profile; blue line, difference. (a) α-MnS NPs from $Mn(Ol)_2$ precursor; (b) 14 nm α-MnS NPs from Mn(OH)(Ol) precursor; (c) MnO NPs.

Table 1. Comparison of the Median Diameter of α-MnS NPs Synthesized by Either Precursor under Otherwise Identical Reaction Conditions[a]

		⟨*d*⟩ (nm)	
T_{ag} (°C)	t_{ag} (min)	Mn(OH)(Ol)	$Mn(Ol)_2$
250	30	9.6	9.3
250	60	10.9	18.1
280	30	11.3	24.9
280	60	11.8	25.6
300	30	13.8	29.5
320	30	14.4	21.1

[a] In all syntheses [Mn] = 0.25 M, S:Mn = 2:1, and the heating rate is 10 °C/min. T_{ag} is the aging temperature and t_{ag} is the aging time.

dipping a tube containing the reaction mixture into a preheated siliconic oil bath. In this way, an average heating rate of ~60 °C/min is achieved (see the Supporting Information). As shown in Figure 3b, such fast heating results in slightly smaller NPs and a similar variation of the $\sigma/\langle d\rangle$ ratio over aging time.

In conclusion, α-MnS NPs are larger when (i) $Mn(Ol)_2$ is used instead of Mn(OH)(Ol), (ii) the aging temperature is higher, and (iii) the heating rate is slower. The duration of the aging period has a scarce effect on the NP size but it is critical to obtain a narrow size dispersion, 30 or 60 min being preferred. However, a narrow size dispersion can be achieved only when the heating rate is at least 10 °C/min.

The dependence of the NP chemical composition on the concentration of sulfur in the reaction mixture was rather unexpected. If one uses a stoichiometric 1:1 S:Mn ratio, the reaction product is a mixture of α-MnS and MnO NPs, no mixed Mn(O,S) NP being formed (see the Supporting Information). To obtain only α-MnS NPs, at least 2 equiv. of sulfur for each equiv. of Mn precursor are required and if 1 equivalent of free oleic acid (OlAc) is added to the reaction mixture, the S:Mn ratio must be at least 3 so to form α-MnS NPs only. Hence, oleic acid (either from the precursor and added as such) scavenges part of the sulfur which is then not available for the growth of Mn sulfide NPs. Because of this interplay between S and OlAc, we could not draw any clear conclusion from α-MnS NP syntheses involving the addition of free OlAc. Finally, when the S:Mn ratio is not higher than 0.6, only MnO NPs are formed.

Synthesis of MnO NPs. Monodisperse NPs of MnO (see Figure 5) could be synthesized using either precursor under typical conditions (see Experimental Section). Again, NPs from $Mn(Ol)_2$ are larger than those from Mn(OH)(Ol), e.g., under typical conditions (absence of S and free OlAc) Mn(OH)(Ol) yields MnO NPs with $<d> = 14.5$ nm and $\sigma = 1.2$ nm, whereas $Mn(Ol)_2$ results in NPs with $<d> = 22.5$ nm and $\sigma = 2.4$ nm. MnO NPs have a hexagonal profile (smoothed in smaller NPs) and form ordered arrays more easily than α-MnS NPs. The ED and XRD patterns in Figures 5 and 2 show that the NPs indeed are fcc MnO. The Rietveld refinement of the XRD profiles was of good quality and yielded crystallite diameters that are in agreement with the values from TEM images.

The effect of adding sulfur or free OlAc to the reaction mixture has been studied using Mn(OH)(Ol) as precursor. Though MnO NPs synthesized in the absence of sulfur have a good dispersion ratio ($\sigma/\langle d\rangle = 8\%$), the latter is further improved when sulfur is added to the reaction mixture, namely $\sigma/\langle d\rangle$ becomes as low as 6% or even 4%, for S:Mn = 0.4 and 0.6, respectively (Figure 5c,d). The NP diameter is conversely not affected by the S:Mn ratio, remaining constant at about 14 nm. The presence of sulfur thus has a significant beneficial effect on the dispersion of MnO nanocrystals. When using the optimal

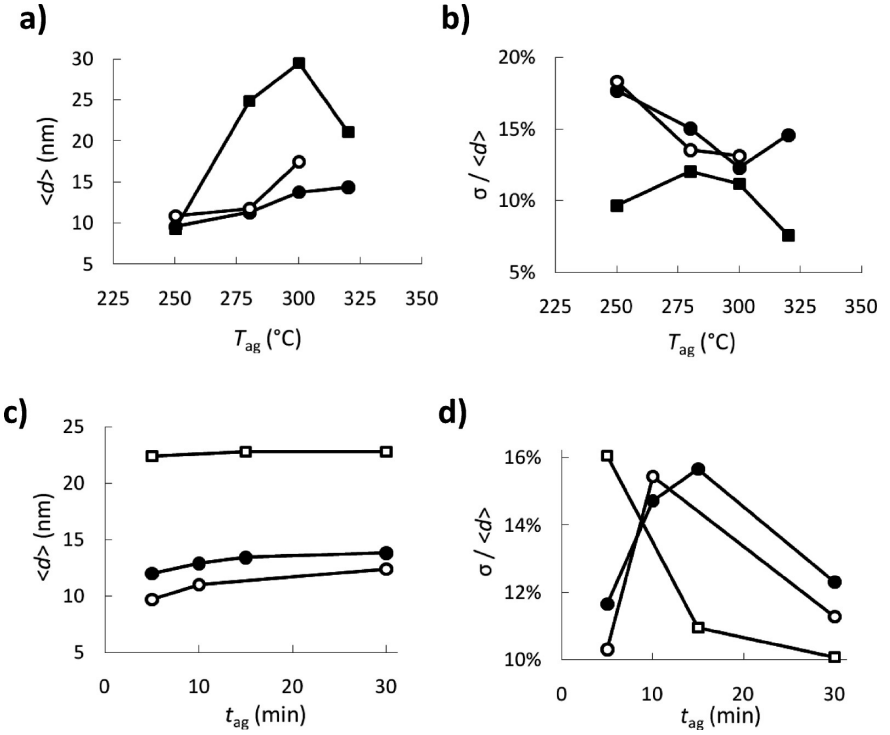

Figure 3. Variation in median diameter $\langle d \rangle$ and dispersion ratio $\sigma/\langle d \rangle$ of α-MnS NPs with (a, b) aging temperature or (c, d) time for selected reaction conditions. The reaction conditions are typical, except when otherwise noted. (a, b) Solid squares, $Mn(Ol)_2$ precursor; solid circles, Mn(OH)(Ol) precursor; open circles, Mn(OH)(Ol) precursor with $t_{ag} = 60$ min (c, d) Open squares: $Mn(Ol)_2$ precursor with $T_{ag} = 320$ °C; solid circles, Mn(OH)(Ol) precursor; open circles, Mn(OH)(Ol) precursor with heating rate ~60 °C/min.

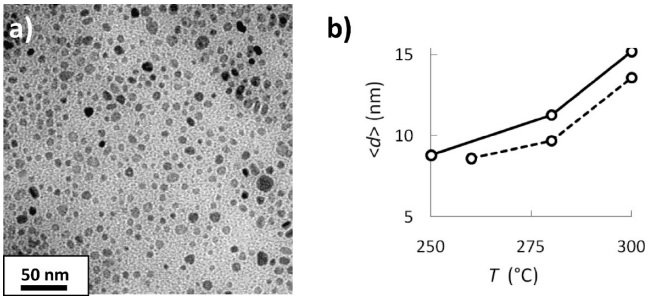

Figure 4. α-MnS NPs formed during the heating step. (a) TEM image of NPs drawn from the reaction vessel at 250 °C during a 5 °C/min heating step; (b) variation of the median diameter $\langle d \rangle$ for heating rate 5 °C/min (broken line) or 3 °C/min (solid line).

S:Mn ratio of 0.6, addition of 0.8 or 1.8 equiv. of free OlAc (with respect to Mn) resulted in MnO NPs with $\langle d \rangle = 19.0$ or 23.6 nm, respectively, values to be compared with $\langle d \rangle = 14.5$ nm for NPs synthesized with no OlAc added (Figure 5e,f). The addition of OlAc does not alter the dispersion, being $\sigma/\langle d \rangle \leq 5\%$ in all cases. Hence, the size of MnO NPs can be conveniently controlled by adding free OlAc to the reaction mixture without affecting their monodispersion.

Shape and Texture. The hexagonal profile of the α-MnS and MnO NPs as seen in TEM images (Figures 1 and 5) suggests that they are not spherical as also hinted by the peculiar pattern displayed where two NP layers are superimposed. Such pattern (e.g., indicated by arrows in Figure 5a,c) is different from the typical hexagonal-compact layering pattern displayed by spherical NPs. In Figure 6 are displayed 14.5 nm MnO NPs arrays formed upon evaporating a drop of NP dispersion on a Formvar/carbon coated grid or on a holey carbon grid. On a flat surface the NPs self-assemble into hexagonal compact arrays and display an hexagonal profile. When deposited on the holey carbon grid, some NPs spontaneously organize into hexagonal compact arrays inside the voids of the carbon film but in these arrays they display a diamond shape. As the superimposed sketches show, these profiles and patterns are evidence that the NPs have octahedral shape, possibly with somewhat smoothed vertices. On the Formvar/carbon-coated grid, the NPs rest with one of the octahedral faces on the grid coating, whereas they set face-to-face when the self-assembled arrays are suspended in the carbon film voids.

Tilted-grid TEM experiments as those shown in Figure 6c,d further demonstrate the octahedral shape of the NPs. The two images display the very same α-MnS NPs as can be appreciated by noticing the NP grouping. Even if these NPs show more of a rounded than a clearly hexagonal profile when seen at 0° tilt (Figure 6c), they have a diamond or rectangular (including square) profile in the image at 36° tilt (Figure 6d). As shown by the sketches at the bottom, these are the profiles expected when octahedral NPs are tilted by 36° about different axes.

In addition to their peculiar shape, both α-MnS and MnO NPs present a strong texture when deposited on a TEM grid. Texture is the nonisotropic distribution of crystallographic orientations in a polycrystalline sample. In NP solid samples, usually obtained by evaporation of a dispersion of nanocrystals, several requisites must be met

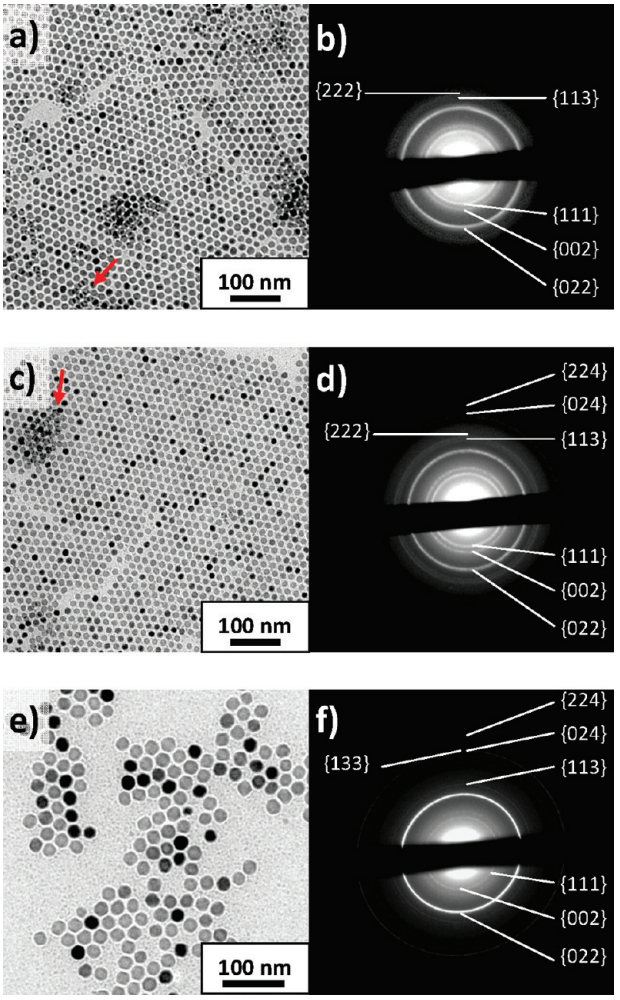

Figure 5. TEM images and indexed diffraction patterns of MnO NPs synthesized using Mn(OH)(Ol) as precursor. (a, b) NPs synthesized in typical conditions; (c, d) NPs synthesized with 0.6 equiv. of sulfur added; (e, f) NPs synthesized with 0.6 equiv. of sulfur and 1.8 equiv. of fre oleic acid added. The red arrows indicate where the peculiar NP superposition pattern is visible.

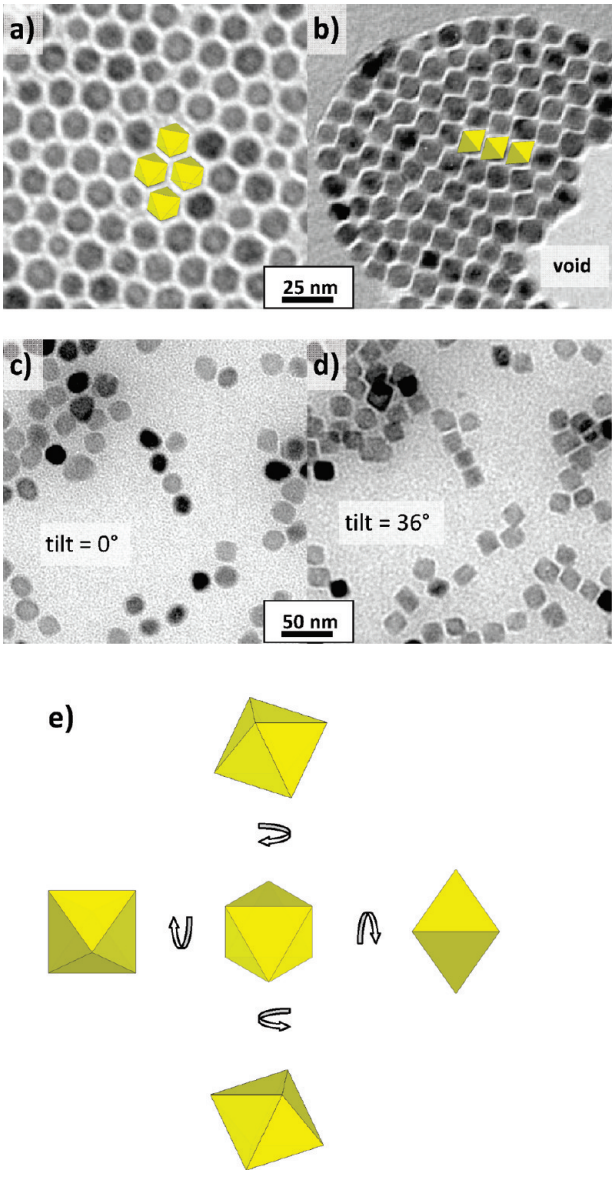

Figure 6. Portraying the shape of MnO and α-MnS NPs. TEM images of 14 nm MnO NPs: (a) array autoassembled on a carbon/Formvar coated grid showing hexagonal profiles; (b) array autoassembled in a void of a holey carbon grid showing diamondlike profiles. TEM images of 25 nm α-MnS NPs: (c) 0° tilt; (d) 36° tilt (tilting axis runs almost horizontally). (e) Sketches showing the possible profiles of an idealized octahedral NP when tilted by 36° about different axis.

in order to develop texture, requisites that regard both the NPs (as for morphology and crystal structure) and the way the sample is prepared. First, the NPs must have a nonspherical shape and their shape must be strictly related to their crystal structure, i.e., the shape must mirror the internal atomic structure. Monodispersion of NP size is not strictly required, but it is necessary to form ordered arrays and thus it is in practice beneficial to the development of texture. Second, the method to form the solid sample (evaporation, precipitation, etc.) must be such that the NPs actually form a textured array.

The latter requirement may seem trivial but, not being met, it prevents texture to be observed in the XRD experiments on our NPs (Figure 2), which possess the morphostructural features required for the development of texture. Indeed, the Rietveld refinement of the XRD profiles was not improved when texture was inserted in the model. The reason is that it is very difficult to achieve a textured NP array large enough to affect the powder XRD recorded with conventional instruments. Conversely, it is easy to create micrometer-sized ordered NP arrays on a TEM grid and strong texture is actually observed by electron diffraction (Figures 1 and 5). The relation between TEM ED pattern, texture and shape is easy to grasp by referring to the first three (and most intense) diffraction peaks of fcc α-MnS and MnO, which, starting from the center of the ring, arise from diffraction by the {111}, {002}, and {022} planes (see Figure 7). Note that the {111} planes coincide with the octahedron faces.

Because the electron wavelength λ is much shorter than the interatomic distances d, by Bragg law ($n\lambda = 2d\sin\theta$) the diffraction angles θ are very small (a few degrees), so that only crystal planes almost parallel to the (vertical) electron beam can diffract electrons.[36] Referring to

(36) Williams, D. B.; Carter, C. B. *Transmission Electron Microscopy*; 2nd ed.; Springer: New York, 2009.

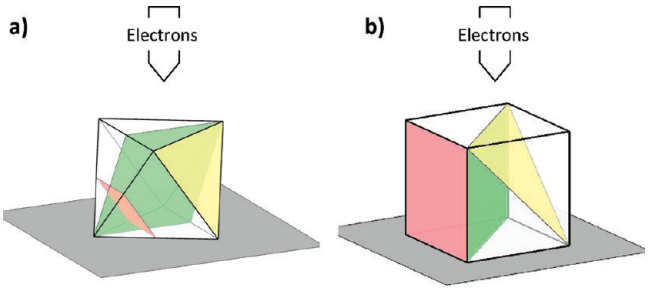

Figure 7. Schematic representation of the main crystallographic planes of crystallites with cubic crystal structure and their geometric relationship with the TEM electron beam in a diffraction experiment. Only one plane of each family of equivalent planes is portrayed. In both pictures, the crystallite rests on the TEM grid upon one of its faces and the electron beam is perpendicular to the grid plane (gray). (a) Octahedral crystallite. The octahedron faces are parallel to the eight {111} planes (yellow), whereas the six {002} planes (red) are parallel to the planes through four vertices and the twelve {022} planes (green) bisect the octahedron passing through two vertices and two edge midpoints. None of the {111} and {002} planes is parallel to the electron beam, whereas three {022} planes are. (b) Cubic crystallite. The cubic faces are parallel to the {002} planes (red), the {111} planes (yellow) are parallel to the planes through three vertices, and the {022} planes (green) bisect the cube passing through four vertices. None of the {111} planes is parallel to the electron beam, whereas four {002} planes (out of 6) and two {022} planes (out of 12) are.

Figure 7, it is easy to see that in octahedral NPs resting on one face, some {022} planes are vertical, and then able to diffract electrons, whereas no {111} and {002} planes are. This is exactly what is observed in the ED experiments (Figures 1 and 5), where the {022} ring is very intense, whereas the {002} and {111} rings are weak or even barely discernible. Such intensity alternation is the well-known signature of {111} texture, i.e., the preferential orientation of crystalline NPs such that one of their {111} planes is perpendicular to the electron beam. The strong {111} texture thus confirms that the NPs have well developed {111} faces on which they rest when deposited on a flat surface. Note that the {111} texture is stronger for larger NPs since they have larger {111} faces and consequently a more precise orientation with respect to the electron beam. Thus, α-MnS and MnO NPs have octahedral shape and the octahedral faces are the {111} planes. The NP faces are thus polar faces composed of Mn cations only (or of anions only), a noteworthy fact because, in vacuum, these faces have much higher energy density than the nonpolar {002} and {022} faces.

Highly Anisotropic Shapes. In particular synthetic conditions α-MnS and MnO NPs with highly anisotropic shapes are obtained, as shown in Figure 8 (Wide-field TEM images can be found in the Supporting Information). When Mn distearate is used as a precursor to α-MnS NPs, very elongated rods or T-shaped NPs with jagged edges are formed (Figure 8a,b) as also previously observed for MnO NPs.[28,37−39] The rods are about 12 nm

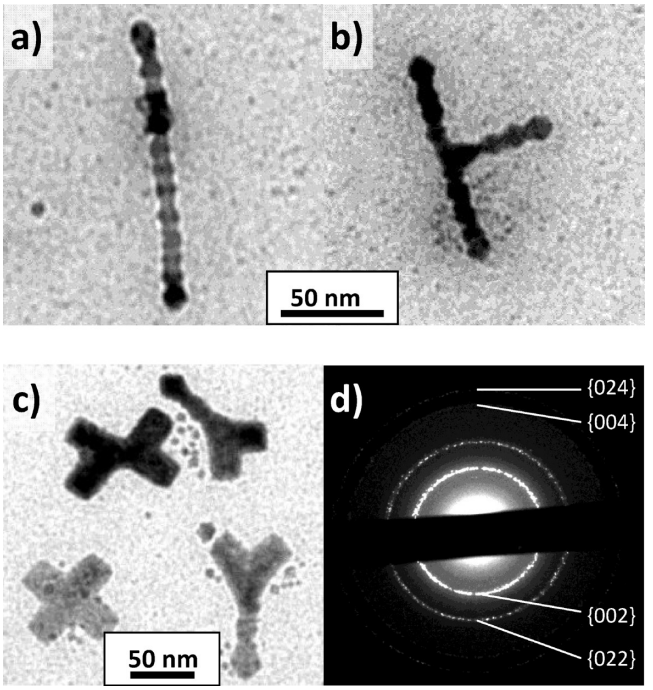

Figure 8. TEM images of α-MnS and MnO NPs with highly anisotropic shapes. (a) Jagged-edge rod and (b) jagged-edge T-shaped α-MnS NPs synthesized using Mn distearate as precursor. (c) Smooth-edge cross-shaped and rod-cross hybrid-shaped MnO NPs synthesized with high concentration of oleic acid, along with (d) their electron diffraction pattern.

wide and have a high aspect ratio (~9). Also, the three T branches are about 12 nm wide and have equal length, suggesting that they grow out from a central core.[38] The edge indentations form a right angle. When a large concentration of oleic acid is present in the reaction mixture for MnO NPs (Mn:OlAc about 1:4), in addition to some rods, other peculiar shapes are observed such as smooth-edged crosses and half-rod half-cross hybrids (Figure 8c). The cross arms form right angles, whereas the angle between the rod and the cross arm in hybrids is 135°. Again, these shapes grow out from a central core with 4-fold symmetry. In the ED pattern of these highly anisotropic NPs (Figure 8d) the {111} ring is absent and the {022} ring has a strongly reduced intensity, in agreement with what expected when the NPs rest on one of the six equivalent {002} faces, i.e., the faces of the cubic crystal cell (Figure 7b). Thus, the highly anisotropic NPs have a {002} texture, as already observed for MnO rods and T-shaped NPs,[38] with part of the {002} and {022} planes vertical. This would also explain the edge angles of these NPs as the angles between {002} and {022} vertical faces. Theory predicts that highly anisotropic NPs are formed when the number of nuclei formed during synthesis is small because of a particularly high activity of the surfactant.[40] In the present case, this occurs when a high Mn:OlAc ratio is used for MnO NPs and when stearic acid is employed instead of OlAc for α-MnS NPs. Interestingly, the high surfactant activity makes the nonpolar faces more stable than the {111} polar faces.

(37) Zitoun, D.; Pinna, N.; Frolet, N.; Belin, C. *J. Am. Chem. Soc.* **2005**, *127*, 15034–15035.
(38) Ould-Ely, T.; Prieto-Centurion, D.; Kumar, A.; Guo, W.; Knowles, W. V.; Asokan, S.; Wong, M. S.; Rusakova, I.; Luttge, A.; Whitmire, K. H. *Chem. Mater.* **2006**, *18*, 1821–1829.
(39) Rusakova, I.; Ould-Ely, T.; Hofmann, C.; Prieto-Centurion, D.; Levin, C. S.; Halas, N. J.; Luttge, A.; Whitmire, K. H. *Chem. Mater.* **2007**, *19*, 1369–1375.
(40) Peng, X. G. *Adv. Mater.* **2003**, *15*, 459–463.

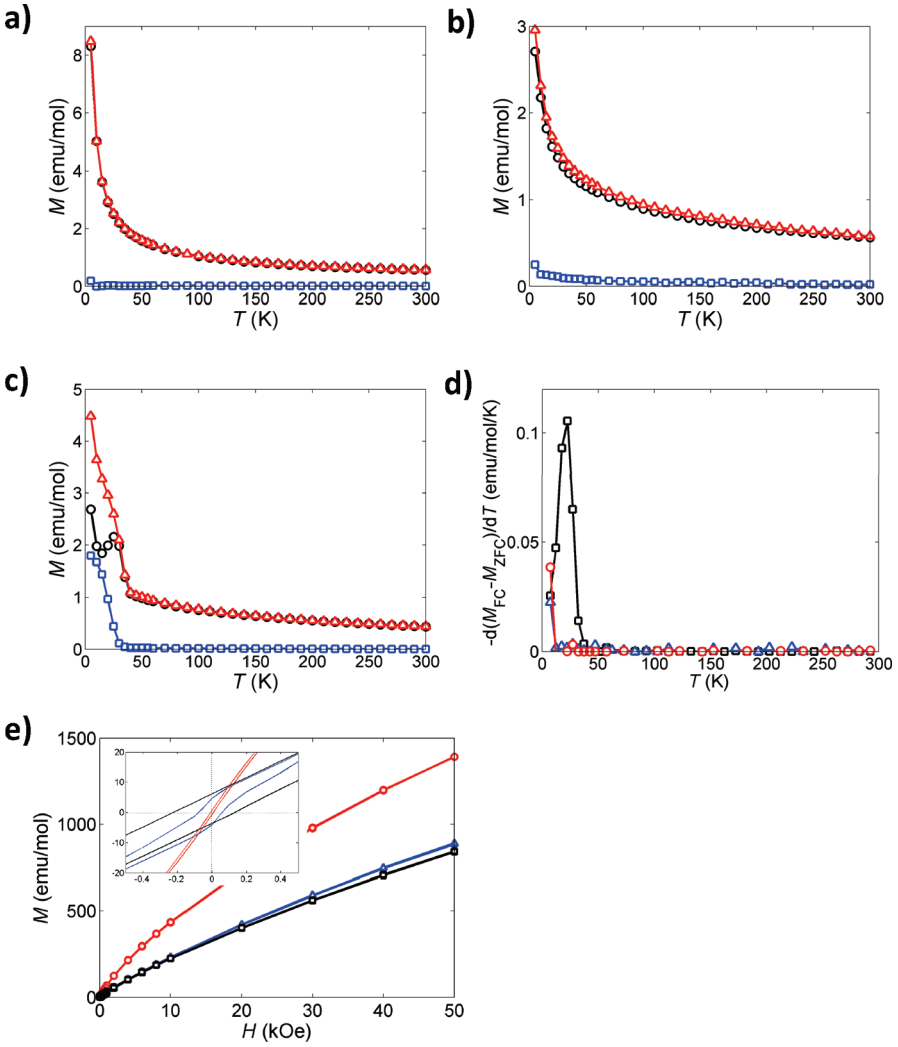

Figure 9. Magnetic properties of α-MnS NPs. (a−c) FC (red triangles) and ZFC (black circles) magnetization and their difference (blue squares) is shown for (a) 14, (b) 20, and (c) 29 nm NPs. (d) Plot of the derivative $-d(M_{FC}-M_{ZFC})/dT$ for 14 (red circles), 20 (blue triangles), and 29 nm (black squares) NPs. (e) Hysteresis of 14 (red circles), 20 (blue triangles), and 29 nm (black squares) NPs; the inset shows the region around zero field.

Magnetic Properties. To the best of our knowledge, the magnetic properties of α-MnS NPs have been investigated only in one case,[1] where different-sized (20−80 nm) α-MnS NPs were AFM with decreased interaction strength in smaller NPs. However, those NPs actually were aggregates of finer particles. We now report on the magnetic properties of single-crystal octahedral α-MnS NPs of different size (14, 20, and 29 nm). The experimental results are shown in Figure 9. The (Z)FC curves of 14 and 20 nm NPs are smooth even if the low-T divergence between ZFC and FC magnetization shows that some irreversible magnetic behavior occurs below 5 and 50 K for 14 and 20 nm NPs, respectively. Conversely, 29 nm NPs show a marked shoulderlike increase in FC magnetization below 50 K and a maximum of the ZFC magnetization at 25 K, which are both evidence of a transition between a superparamagnetic (SPM) and a blocked state possessing order of ferromagnetic (FM) type. The presence of FM-like regions in 29 nm NPs is also clearly visible in the magnetization difference curve (Figure 9c). Such behavior is confirmed by the data in Figure 9d, where the derivative of the difference between ZFC and FC magnetization is plotted as a function of temperature. Such plot actually reflects the distribution of energy barriers which prevent magnetization flips in the FM-like blocked state,[41] i.e., such a plot portrays the distribution of the blocking temperatures[42] in the sample. Clearly, 29 nm α-MnS NPs undergo a transition between a blocked and a SPM state with a mean blocking temperature of 23 K and a narrow distribution of energy barriers. A similar transition might be present a $T \leq 5$ K for 14 and 20 nm NPs.

In all cases, the magnetic behavior at $T > 50$ K is reversible and the high-T magnetization data can be fitted to the Curie−Weiss law[43] $\chi = C/(T - \Theta)$ where χ is the susceptibility, Θ is the Curie−Weiss temperature, and C is a constant proportional to the square of the effective magnetic moment p_{eff} of Mn ions. The best-fit Curie−Weiss temperatures, reported in Table 2, are negative indicating

(41) Rondinone, A. J.; Samia, A. C. S.; Zhang, Z. J. *J. Phys. Chem. B* **1999**, *103*, 6876–6880.
(42) Dormann, J. L.; Fiorani, D.; Tronc, E. *Adv. Chem. Phys.* **1997**, *98*, 283–494.
(43) Aharoni, A. *Introduction to the Theory of Ferromagnetism*; 2nd ed.; Oxford University Press: Oxford, U.K., 2000.

Table 2. Magnetic Properties for Different-Sized Octahedral α-MnS NPs[a]

$\langle d \rangle$ (nm)	Θ (K)	p_{eff} (μ_B)	H_e (Oe)	H_c (Oe)
14	−149	4.6	0	9
20	−227	4.8	−17	81
29	−272	4.9	−44	180

[a] Curie−Weiss temperature Θ and effective magnetic moment p_{eff} are best-fit values to the Curie−Weiss law. Exchange-bias H_e and coercive H_c field are measured by FC hysteresis experiments at 5 K.

that the NPs are AFM. The Θ values are less negative than the bulk value[44] of −465 K and approach this value as they become larger. Then, the AFM interactions become less effective for smaller NPs, in qualitative agreement with previous results.[1] The effective moments are close to the bulk value[45] of 4.54 μ_B.

The hysteresis of octahedral α-MnS NPs measured at 5 K after FC at 50 kOe (Figure 9e) shows that the NPs are far from being magnetically saturated even at 50 kOe. More interesting is the behavior near zero field (see inset). All NPs show a small coercive field, larger for larger NPs, and the hysteresis of 20 and 29 nm NPs is shifted by a bias field of −17 and −44 Oe, respectively. The presence of coercivity indicates that at low temperature some FM-like order is present in the NPs and, more interestingly, the presence of a bias field is evidence of exchange coupling across a FM-AFM interface.[46] The magnetic data thus indicate that single-crystal octahedral α-MnS NPs have a magnetic core−shell structure[47] comprising two regions: (i) a core where the main interactions between spins are AFM, though weaker than in the bulk, and (ii) a shell comprising uncompensated spins that are in the SPM regime at high T and undergo a transition to a FM-like blocked state at low T. Exchange interactions are effective across the AFM/FM core−shell interface. In smaller particles the energy barrier for the SPM/blocked transition are lower and hence the exchange bias at a given T is less effective.

Conclusions

Investigation of the synthesis of α-MnS and MnO NPs by the decomposition of manganese mono- or dioleate in octadecene at high temperature in the presence of elemental sulfur led to the following conclusions. Both precursors yield monodisperse octahedral α-MnS or MnO NPs when decomposed at high temperature (250−300 °C) in octadecene. Unexpectedly, to produce pure α-MnS NP samples a S:Mn ratio of (at least) 2:1 is required, whereas using a stoichiometric 1:1 S:Mn ratio produced a mixture of α-MnS and MnO NPs, and pure MnO NP samples were obtained when S:Mn ≤ 0.6. Such effective sulfur depletion is ascribed to oleic acid, either from the precursor and added to the reaction mixture.

The main difference between $Mn(Ol)_2$ and Mn(OH)(Ol) is that they yield NPs in significantly different size ranges, Mn(OH)(Ol) giving NPs about half in size than those produced from $Mn(Ol)_2$ under the same conditions. For instance, at 300 °C Mn(OH)(Ol) gave 14 nm α-MnS and 14 nm MnO NPs, whereas $Mn(Ol)_2$ yielded 30 nm α-MnS and 23 nm MnO NPs. This difference is related to the different amount of oleic acid present in the reaction mixture, since by adding free oleic acid in the synthesis of MnO NPs from Mn(OH)(Ol), NPs as large as 24 nm were obtained. These results can be explained in the framework of the theory proposed by Chen et al.[28] in relation to the synthesis of MnO NPs from $Mn(St)_2$. Their data could be explained assuming that the stearic acid liberated by the precursor decomposition is able to dissolve smaller NPs reconstituting new precursor which enables larger NPs to grow further. In our case, which is chemically very similar to their one, such a dissolution−growth mechanism is more efficient when $Mn(Ol)_2$ is involved (or when free acid is added to the reaction mixture) because of the larger effective concentration of oleic acid, thus yielding larger NPs.

Beside the choice of the precursor, control over NP size and dispersity is afforded by varying aging temperature, aging time, and heating rate. The size of α-MnS NPs from $Mn(Ol)_2$ could be regulated between 18 and 30 nm, and that of NPs from Mn(OH)(Ol) between 10 and 14 nm. As mentioned above, size control of MnO NPs is also possible by addition of free oleic acid.

TEM experiments, including tilting, evidenced that α-MnS and MnO NPs have octahedral shape. Thanks to this shape, ordered arrays of NPs obtained on TEM grids show a strong texture along the {111} direction, as evidenced by electron diffraction. Finally, α-MnS NPs have a magnetic core−shell consisting of an antiferromagnetic core and a ferromagnetic-like shell that are exchange coupled below the blocking temperature of the shell (23 K for 29 nm α-MnS NP).

Acknowledgment. Financial support from Regione Lombardia (Italy) within the "Mind in Italy" initiative and from the Fondazione Cariplo (Milano, Italy) under Grant 2004-1154 is gratefully acknowledged. We thank Dr. M. Gemmi for HRTEM micrographs and Dr. Ilenia Rossetti for powder X-ray diffractograms.

Supporting Information Available: Elemental analysis, infrared and ESI-MS spectra of manganese precursors; temperature vs time plot for dipping the reaction tube in a hot oil bath; electron diffractogram of a mixed α-MnS and MnO NP sample; TEM images of α-MnS and MnO NPs with highly anisotropic shapes (PDF). This material is available free of charge via the Internet at http://pubs.acs.org.

(44) Corliss, L.; Elliott, N.; Hastings, J. *Phys. Rev.* **1956**, *104*, 924–928.
(45) Pearce, C. I.; Pattrick, R. A. D.; Vaughan, D. J. *Sulfide Mineral. Geochem.* **2006**, *61*, 127–180.
(46) Nogués, J.; Sort, J.; Langlais, V.; Skumryev, V.; Suriñach, S.; Muñoz, J. S.; Baró, M. D. *Phys. Rep.* **2005**, *422*, 65–117.
(47) *Surface Effects in Magnetic Nanoparticles*; Fiorani, D., Ed.; Springer: New York, 2005.